metals

MDPI

Article

Effect of Ultrasound on Microstructure and Properties of Aluminum–Copper Friction Stir Lap Welding

Wenzhen Zhao [1], Yalong Zhu [1], Zhaoxian Liu [1], Xiaoyang Yi [1], Jian Wang [2], Ao Fu [2], Fengyi Wang [3,*] and Huan He [1,*]

[1] School of Nuclear Equipment and Nuclear Engineering, Yantai University, No. 30, Qingquan Road, Laishan District, Yantai 264005, China; zhaowenzhen@ytu.edu.cn (W.Z.); nby10032@s.ytu.edu.cn (Y.Z.); zhaoxina98@s.ytu.edu.cn (Z.L.); yixiaoyang@ytu.edu.cn (X.Y.)
[2] State Key Laboratory of Powder Metallurgy, Central South University, Changsha 410083, China; 213307006@csu.edu.cn (J.W.); aofu_ice@csu.edu.cn (A.F.)
[3] School of Materials Science and Engineering, Wuhan University of Technology, Wuhan 430070, China
* Correspondence: wfy1989@whut.edu.cn (F.W.); hehuan@ytu.edu.cn (H.H.)

Abstract: In this paper, the influence mechanism of ultrasound on plastic flow and microstructure features of the aluminum–copper friction stir lap welding (Al/Cu-FSLW) process is systematically investigated by adjusting the welding speed and improving the shear rheology in the plastic stirring zone. Through adjusting the ultrasonic vibration and welding speed, the directional control of mechanical properties is realized. It is found that increasing the welding speed properly is beneficial to enhance the mechanical shear between the tool and the workpiece, thus forming more staggered layered structures at the copper side and improving the tensile strength of the weld. The acoustic softening enhances the viscoplastic fluid mixing and strengthens the mechanical interlock of the Al/Cu lap interface. As the welding speeds increase or ultrasonic vibration is applied, the thickness of Al/Cu intermetallic compound (IMC) decreases, and the tensile strength and elongation of the Al/Cu joints are enhanced. Compared with adjusting the welding speed, the ultrasonic vibration can further refine the copper particles which are stirred into the plastic zone, and the thinning effect of ultrasound on IMC layers is better than that of increasing welding speed. At the welding speed of 60 mm/min, the IMC layer thickness is reduced by 42% under ultrasonic effect. In three welding speed conditions, the UV reduced the absolute value of the effective heat of formation (EHF) for Al_2Cu and Al_4Cu_9 and suppressed the formation of AlCu phase. Meanwhile, only when the welding speed is increased from 60 mm/min to 100 mm/min can the formation of AlCu be suppressed. Under the ultrasonic optimization, the stable improvement of welding efficiency is ensured.

Keywords: Al/Cu dissimilar alloys; friction stir lap welding; ultrasonic vibration; welding velocity; intermetallic compounds; plastic flow

Citation: Zhao, W.; Zhu, Y.; Liu, Z.; Yi, X.; Wang, J.; Fu, A.; Wang, F.; He, H. Effect of Ultrasound on Microstructure and Properties of Aluminum–Copper Friction Stir Lap Welding. *Metals* **2024**, *14*, 1162. https://doi.org/10.3390/met14101162

Academic Editor: António Bastos Pereira

Received: 11 September 2024
Revised: 5 October 2024
Accepted: 9 October 2024
Published: 11 October 2024

1. Introduction

Aluminum–copper composite structures have excellent electrical conductivity and good economy and are widely used in the aerospace field and the manufacture of electrical equipment [1–3]. However, the huge differences in thermal and mechanical properties between aluminum alloy and copper make it quite difficult to connect them through fusion welding. And due to the high surface brightness of copper, it is also challenging to use fusion welding methods with high energy density, such as laser welding [4,5]. Solid-state welding processes with low heat input, and with no need to melt materials, such as ultrasonic welding, friction welding, and friction stir welding (FSW), have obvious advantages in welding aluminum and copper. Solid-phase welding uses plastic deformation at local high temperature and high strain rate to realize effective combination and can generate less brittle-hard Al/Cu-IMC under low heat input and is more suitable for Al/Cu joining [6–9]. Compared with ultrasonic welding, the FSW process can achieve a larger process window

and a wider range of plate thickness, so it has a better industrial prospect for the welding of dissimilar materials of aluminum alloys and copper.

During the FSW process, the workpieces undergo the strong shearing action of the tool, and the local rapid rise in temperature and material softening are realized by the mutual friction between the tool and the workpiece. The mechanical interlocking and metallurgical bonding of dissimilar Al/Cu materials are realized with the shear rheology under high strain rate [10–12]. For the Al/Cu-FSLW process, researchers mostly consider the placement of materials, the configuration of welding speed and tool rotating speed, the shape and structure design of the tool, and the auxiliary energy field or intermediate layer transition [13–15]. When thin plates of aluminum alloys and copper are joined with the FSLW process, Zn foil is often used as the intermediate layer to reduce the brittle IMCs. Li et al. [16] added Zn as an intermediate layer and they found that a soft IMC layer composited with Cu/Zn was generated, improving the mechanical properties of Al/Cu joints. In addition to using Zn foil alone as the intermediate layer, researchers also found that SiC can be used as the intermediate layer, or other composite welding processes can be superimposed. Maity et al. [17] used SiC particles as the interlayer, and they proved that the peel strength was improved by 70% without affecting the joint resistance. Based on the addition of a zinc intermediate layer, Tong et al. [18] combined it with the self-reactive brazing mechanism, and they also improved the fracture resistance of the Al/Cu joint by 59%. Paidar et al. [19] combined the technology of friction spot extrusion welding–brazing with a Zn intermediate layer, and they found the keyhole was eliminated totally. Furthermore, the weld strength and elongation of the joint were significantly improved. However, the method of adding an intermediate layer is more suitable for thin plates and short pins. For the lap joint of medium-thickness plates, it is necessary to ensure sufficient plastic flow of the bottom copper plate and also the plastic mixing of aluminum with the copper. So, it is necessary to optimize the process from the perspective of strengthening plastic deformation.

A large number of studies have confirmed that optimizing the tool design [20–23] and adding energy field assistance [24–27] can effectively improve the plastic flow during the FSW process. In the investigation of the effect of tool design on the plastic flow and microstructure in the weld nugget, Xie et al. [28] found that the increase in thread depth can promote the dynamic recrystallization and improve plastic deformation. Based on the promotion of ultrasonic vibration to metal plastic deformation, a variety of ultrasonic coupling processes have been developed in the research of process modification of the friction stir welding process. Moreover, a lot of basic research has been carried out on ultrasonic-assisted friction stir welding of aluminum alloy, aluminum–magnesium alloy, aluminum steel, and aluminum–copper. Zuo et al. [29] proposed an ultrasound-assisted friction stir transient liquid phase spot welding process, and they found that the application of ultrasonic vibration could break IMC particles and thicken the eutectic layer. He et al. [30] applied ultrasonic vibration to the tool. They found that the distribution uniformity of IMCs and the tensile strength of the weld were significantly improved when the ultrasound was coupled with the tool. Karrar et al. [31] found that the increasing of the rotating speed could promote mechanical interlocking, but also the heat input could increase, which promoted the generation of IMCs. You et al. [32] found that the application of ultrasonic vibration can transfer the tensile fracture position to the non-interface, thus improving the tensile strength of the Al/Cu joints. Su et al. [33] found that the distribution uniformity of IMCs was improved and the thickness of IMCs in the Al/Cu interface was reduced after the application of ultrasound. Chowdhury et al. [34] proposed that ultrasound can provide energy for the welding process and contribute to the reconstruction of metal grains. Thoma et al. [35] found that ultrasound can compensate the heat source required for welding and act as external mechanical energy to inhibit IMC growth in ultrasonic-assisted FSW research of Al/steel. The investigations of joining of dissimilar metals by ultrasonic-assisted FSW processes show that the acoustic softening effect will reduce the plastic deformation

resistance, even the plastic difference between dissimilar materials, and it further reduces the welding load and improves the mechanical properties of the joint.

However, at present, few studies have considered the application of ultrasound to the Al/Cu heterogeneous FSW process. Moreover, there is a lack of systematic research on the matching relationship between welding parameters and ultrasonic effect. In order to deeply study the ultrasonic influence mechanism and adjust the adaptability of ultrasound and welding parameters, the effects of ultrasound on the formation and growth of Al/Cu-IMC and the plastic flow of the weld nugget under different welding speeds were compared and analyzed in this paper. The distribution morphologies of IMCs, the phase composition of intermetallic compounds, and mechanical properties of joints under different welding speeds and with or without ultrasonic assistance were compared and analyzed. The influence mechanism of both welding speed and ultrasonic vibration assistance on Al/Cu friction stir lap welding was revealed from the point of view of the effective heat of IMC formation.

2. Experimental Procedure

The ultrasonic application method and the schematic diagram of the ultrasonic-assisted friction stir lap welding (UFSLW) process are shown in Figure 1. AA6061-T6 aluminum alloy and copper plate were lapped, and the workpieces were both 150 mm (length) × 75 mm (width) × 3 mm (height). The aluminum plate was placed on the top and the copper was placed on the bottom. The ultrasonic device was fixed on the spindle and moved synchronously with the tool. The selection of tool rotating speed and the welding speeds was based on the principle of no defects in the joint and presenting the most significant ultrasonic effects. As shown in Figure 1, the tool rotates counterclockwise at 800 rpm. The welding speed was 60 mm/min, 80 mm/min, and 100 mm/min, respectively. And the tilt angle of the tool is 2.5°. A conical pin was adopted. The diameter of the shoulder of the tool is 12 mm. And the diameters at the tip and root of the pin are 3.2 mm and 4.6 mm. The length of the pin is 3 mm. And the plunge depth of the pin was 0.2 mm. The ultrasonic horn was directly applied on the top surface of the aluminum and located 28 mm in front of the tool. The ultrasonic vibrating frequency was 20 KHz, and the ultrasonic amplitude was 20 μm.

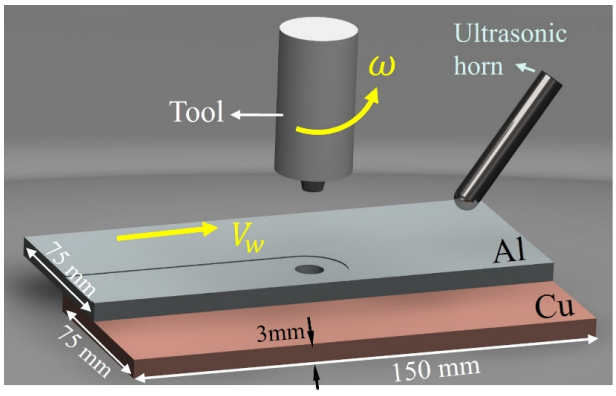

Figure 1. The schematic diagram of ultrasonic-assisted friction stir lap welding (UFSLW) process.

After the welding experiment, the weld cross-sections under different parameters for FSLW and UFSLW were taken to prepare the metallographic samples. In order to observe the boundary of the thermomechanically affected zone (TMAZ), the aluminum side was corroded by Keller reagent for 15 s. The copper side was corroded by a mixed reagent (ammonia:hydrogen peroxide:water = 5:2:5) for 20 s. And the boundaries of the TMAZ of samples under different welding speeds with or without ultrasonic vibration were photographed via stereomicroscopy. On the lap interfaces of aluminum and copper, the typical locations were observed by metallographic microscopy and scanning electron microscopy (SEM) to compare the morphologies and distributions of IMCs. After welding, wire cutting

sampling was adopted for samples in the middle position of the weld perpendicular to the welding direction. Three groups of parallel tests were conducted for each group of welding parameters, and the test results were averaged. The tensile specimen size was 40 mm × 20 mm × 3 mm, and the shear resistance of the lap joint was tested by a CMT5105 tensile testing machine (Suns Co., Ltd., Shenzhen, China) at room temperature. The strain rate is 1mm/min. The microhardness of the aluminum–copper lap joint was tested by a Huayin microhardness tester (HV-1000A, Laizhou Huayin Test Instrument Co., Ltd., Yantai, China), and the load was 50 gf. And the distance between consecutive indents was 0.5 mm.

3. Experimental Results and Analysis

3.1. Ultrasonic Effect on Plastic Flow of Al/Cu Joint

Both ultrasound and the welding speed have a direct impact on the plastic flow at the Al/Cu lap interface, and the macroscopic pictures of the weld cross-sections under different welding speeds of FSLW and UFSLW processes were selected for comparative analysis, as shown in Figure 2. Figures 2a–c and 2d–f are the cross-sectional morphologies of FSLW and UFSLW processes at welding speeds of 60 mm/min, 80 mm/min, and 100 mm/min, respectively. Under the mechanical shearing and strong disturbance of the tool, the copper was plastically deformed and the inverted hook-shaped Al/Cu interfacial lock and morphology were formed on the retreating side (RS). Affected by material viscosity, strain rate, interfacial stress state, and material thermophysical properties, with the increase in welding speed, the residence time of the tool in the stirring zone decreases, and the disturbance effect on plastic flow of material in the shear layer decreases. Therefore, the intensity of plastic flow decreases, which will lead to a decrease in viscous heat in the shear layer.

And as the welding speed increased, the height of the hook also increased. The reason is that the local heat generation and plastic softening were higher under the 60 mm/min welding speed. At 100 mm/min, the frictional shear stress was dominant at the tool/workpiece contact interface, which made the mechanical shearing action of the tool more intense and resulted in a sharper shape of hooks. After the ultrasonic action was superimposed, the hook-shaped morphology went deeper into the aluminum side. In order to observe the distribution morphology of the aluminum–copper interface in detail to further compare the ultrasonic action on the plastic flow, three typical positions were selected in six groups of cross-sections, and the metallographic diagrams are shown in Figure 3.

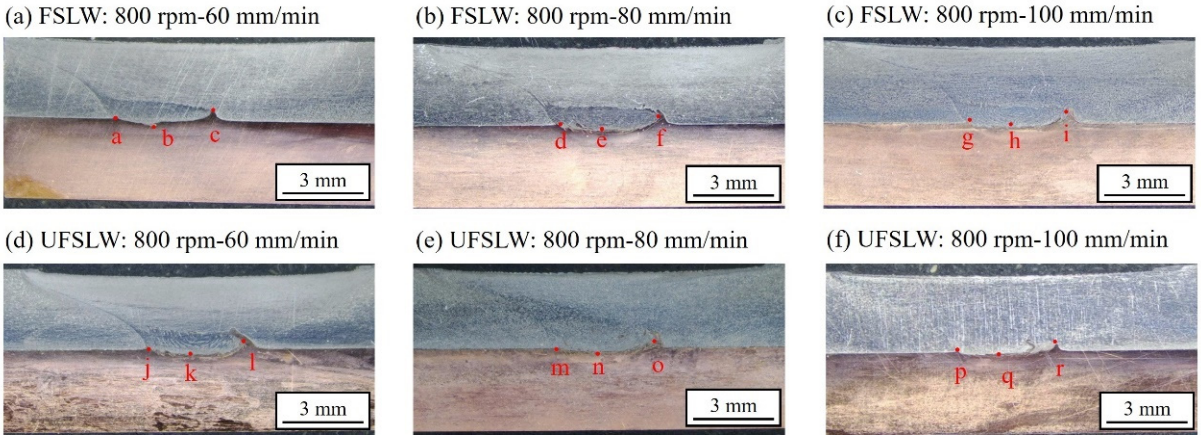

Figure 2. Morphological comparison of weld cross-sections at different welding speeds. (**a**) 800 rpm, 60 mm/min, FSLW, (**b**) 800 rpm, 80 mm/min, FSLW, (**c**) 800 rpm, 100 mm/min, FSLW, (**d**) 800 rpm, 60 mm/min, UFSLW, (**e**) 800 rpm, 80 mm/min, UFSLW, (**f**) 800 rpm, 100 mm/min, UFSLW. Red letters marked the typical positions selected in six groups of cross-sections, and the partially enlarged metallographic diagrams was shown in Figure 3.

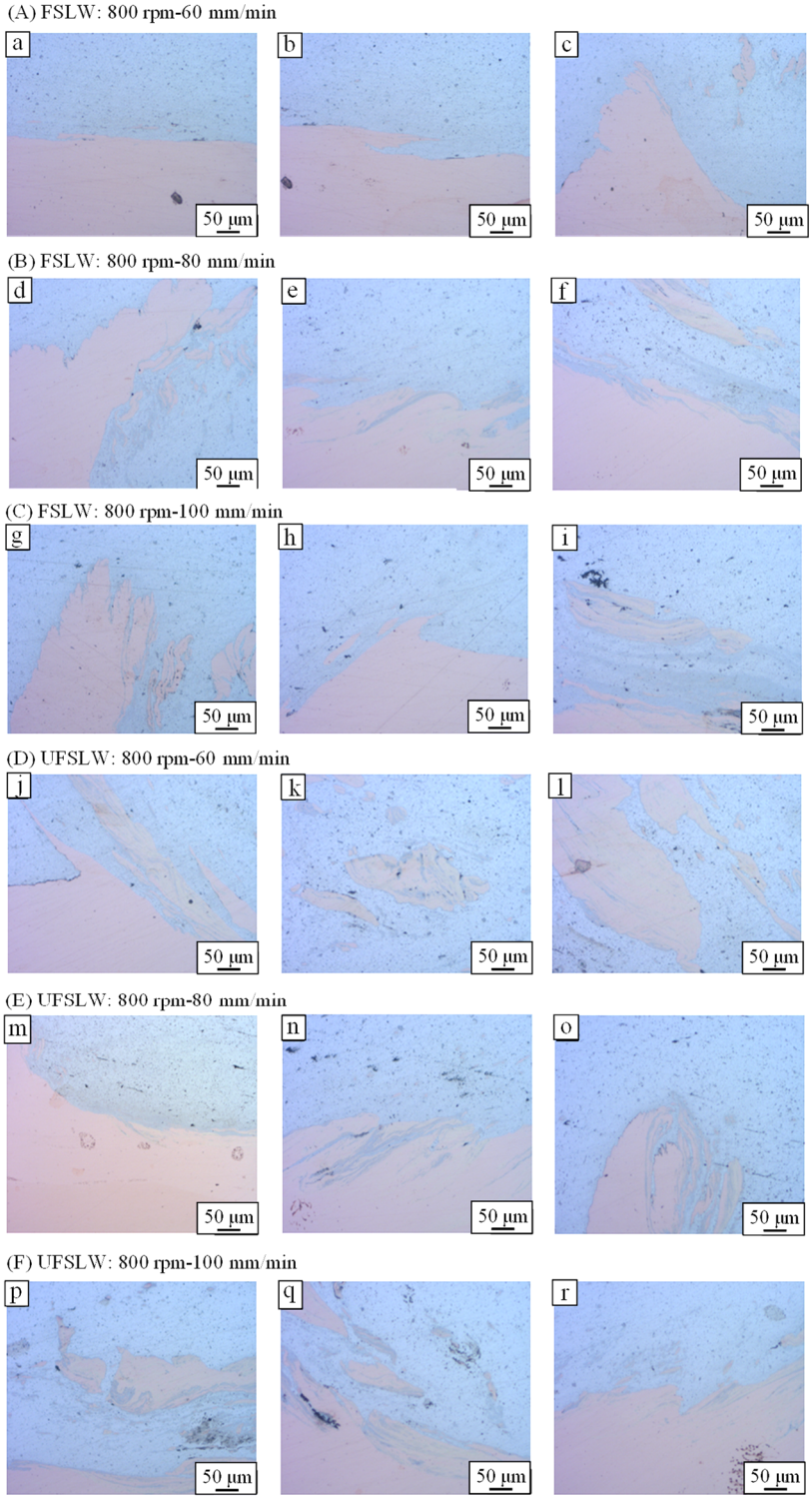

Figure 3. Metallographic microstructures at the Al/Cu interface of the welding parameter at different welding speeds. (**A**) 800-60-FSLW, (**B**) 800-80-FSLW, (**C**) 800-100-FSLW, (**D**) 800-60-UFSLW, (**E**) 800-80-UFSLW, (**F**) 800-100-UFSLW. The serial numbers a~r corresponding to the typical positions selected in Figure 2.

The plastic flow between aluminum and copper was not harmonious because of their different plasticity, and a large number of layered structures were formed on the copper side. With the application of ultrasound, it can be clearly seen in Figure 3 that the mechanical interlocking structure with staggered aluminum and copper layers increased.

The copper particles/blocks entering the aluminum side were further refined and dispersed under the ultrasonic softening effect. This indicated that ultrasound promoted the plastic deformation of the underlying copper and reduced the deformation resistance. It can also be noted that increasing the welding speed properly is beneficial to form more staggered layered structures at the copper side, which indicated the mechanical shear between the tool and the workpiece was enhanced. Because the hook morphology can more directly reflect the flow state of the aluminum–copper lap interface, Figure 4 further shows the microscopic scanning diagram corresponding to the hook positions under welding speeds of 60 mm/min, 80 mm/min, and 100 mm/min.

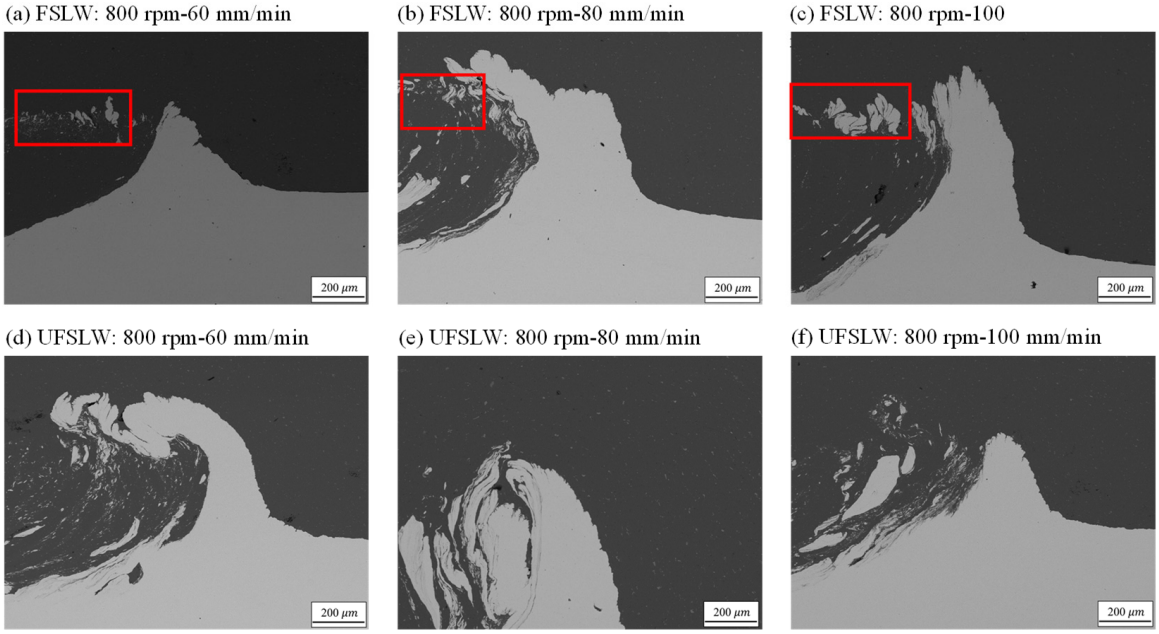

Figure 4. SEM images showing the morphologies of the hooks at different welding speeds on the Al/Cu lap interfaces. (**a**) 800 rpm, 60 mm/min, FSLW, (**b**) 800 rpm, 80 mm/min, FSLW, (**c**) 800 rpm, 100 mm/min, FSLW, (**d**) 800 rpm, 60 mm/min, UFSLW, (**e**) 800 rpm, 80 mm/min, UFSLW, (**f**) 800 rpm, 100 mm/min, UFSLW. In the red box are copper particles/blocks in the nugget area.

From the nugget area near the hook, it can be found that copper particles/blocks entering the aluminum matrix were dispersed in the stirring area. In Figure 4a–c, with the decrease in welding speed, the size of copper particles/blocks entering the aluminum side became smaller, showing a more uniform dispersion distribution. In the area marked by the red box in Figure 4, it can be seen that the size and distribution of copper particles/copper blocks in the nugget zone are obviously different at different welding speeds. In Figure 4a, the copper in the stirring zone is distributed in particles. The large copper particles are about 55.85 μm long and 121.62 μm wide, while the small ones are about 20.65 μm long and 20.11 μm wide. The distribution is more uniform and dispersed. With the increase in welding speed, at 80 mm/min, copper is mainly distributed in large particles. The size of large particles is about 89.78 μm long and 94.86 μm wide. When the welding speed is increased to 100 mm/min, the distribution morphology of copper in the nugget zone is mainly copper blocks, among which the larger copper blocks are 118.61 μm long and 156.47 μm wide, and the smaller particles are about 63.66 μm long and 46.58 μm wide.

According to the size and morphology of copper particles/blocks distributed in the nugget zone, the welding speed has a great influence on the migration and plastic flow of aluminum–copper materials. At the welding speed of 60 mm/min, the welding heat generation was higher than that of 80 mm/min or 100 mm/min. The plastic deformation of copper was more intense, and local plastic softening in the shear layer was more sufficient. Therefore, the pin plays a stronger role in promoting the flow and migration of copper

matrix. Moreover, under the strong stirring action, the fully softened copper enters the nugget area on the aluminum side in the form of fine particles, is dispersed with the rotation and forward movement of the pin, and is evenly distributed in the onion ring. When the welding speed is high, the copper matrix is not fully softened, and the shear action of the pin makes the local copper block peel off, so that the granular dispersion distribution cannot be achieved, and its plastic flow stops. Therefore, at the welding speeds of 80 mm/min and 100 mm/min, copper particles in the nugget area become larger and copper blocks appear.

The height and width of hook morphology were measured, as shown in Table 1. The results show that, for the FSLW process, with the increase in welding speed, the size of hooks increased gradually. When the welding speed was increased to 100 mm/min, the height and width of hooks were increased by 35.7% and 58.7%, respectively, compared with 60 mm/min. The results show that the increase in welding speed will weaken the local plastic softening degree and reduce the plastic flow of copper. At the welding speed of 60 mm/min, the copper at the hook tip was fully softened, was dispersed by the pin, and entered the nugget area. Therefore, the hook size was small. However, at 100 mm/min, the plastic softening degree of copper was low. After the hook morphology was embedded in the aluminum side under shear stress, the tool left and the plastic flow of copper was stopped, so the hook size was larger.

Table 1. Width and height of hooks under different welding parameters.

Welding Process	Width (mm)	Height (mm)
800-60-FSLW	0.54	0.42
800-80-FSLW	0.73	0.51
800-100-FSLW	0.857	0.57
800-60-UFSLW	0.886	0.726
800-80-UFSLW	0.63	0.6
800-100-UFSLW	0.456	0.23

However, after ultrasonic application, the acoustic softening effect compensated for the lack of local softening degree when the welding speed was increased. Under the condition of sufficient softening, more copper entered into the nugget zone, and less copper remained at the hook position. With the increase in welding speed, the hook size gradually decreased. Under the coupling effect of low welding speed of 60 mm/min and ultrasonic softening, the softening effect of the pin on bottom copper was significantly higher than that of other welding parameters, so the shear effect of the tool on fully softened plastic copper material made the size of hook morphology reach its peak value.

3.2. Ultrasonic Effect on Microstructure and IMC Growth

The formation of brittle-hard-phase Al-Cu compounds will affect the mechanical properties of the joint. A uniform distribution with thin Al/Cu-IMCs is beneficial to the comprehensive properties of the joint. In this section, SEM images of IMC morphology and distribution at Al/Cu lap interfaces are shown to analyze the order of compound formation and ultrasonic mechanism.

As shown in Figure 5, the morphologies of the Al/Cu-IMCs on the Al/Cu interfaces under different welding speeds of FSLW and UFSLW processes are compared. With the increase in welding speed, the total thickness of IMCs gradually decreased. For the FSLW process, it was clear that the IMCs formed three layers at the welding speeds of both 60 mm/min and 80 mm/min. When the welding speed was increased to 100 mm/min, the IMC layers were reduced to two. At 60 mm/min, the boundary of the IMC layer had a sawtooth shape, the thickness was uneven, and the distribution morphology changed greatly. Meanwhile, in Figure 5d–f, only two layers of IMCs appeared the three welding speeds when the ultrasonic assistance was applied. Compared with the same welding speeds of the FSLW process, ultrasound reduced the total thickness of IMCs. And the

boundaries of IMC layers were straighter and the distribution morphologies were more uniform. Therefore, it can be concluded that ultrasound and the increase in welding speed could both improve the uniformity and continuity of the IMC layer significantly. But ultrasonic assistance plays a more significant role in thinning and reducing the Al/Cu-IMCs. The reason is that the increasing welding speed and application of ultrasonic vibration could both reduce the heat generation and the temperature in the nugget zone [36], which could further inhibit the generation of IMCs.

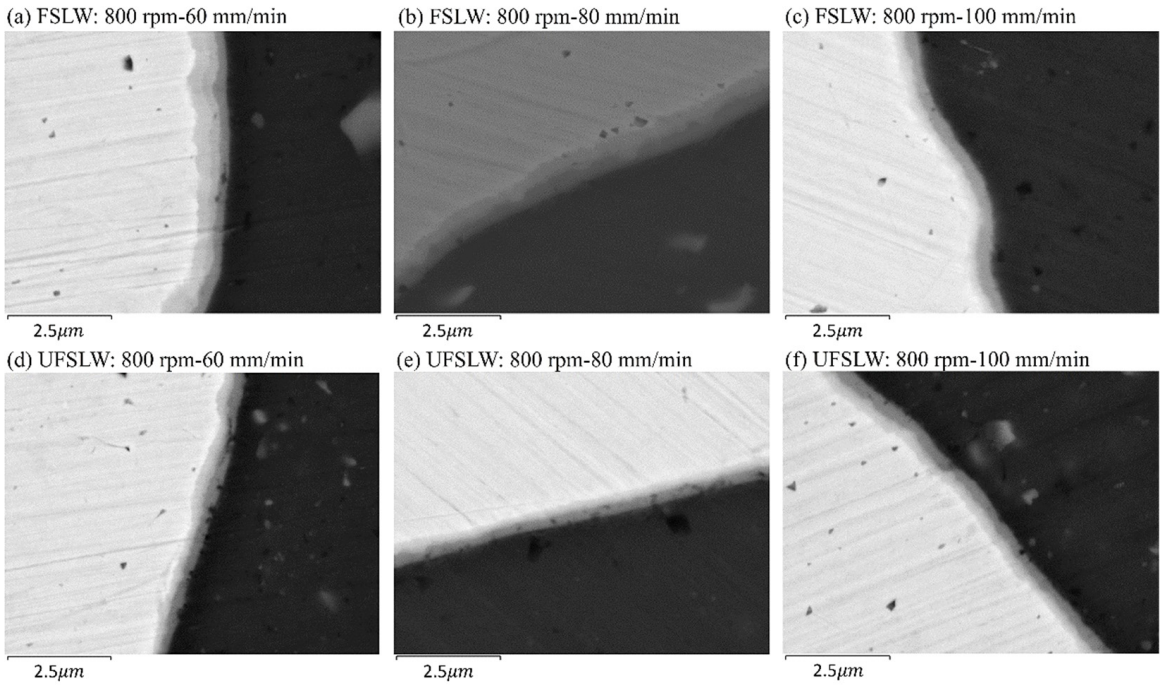

Figure 5. SEM image showing the distribution and morphologies of the Al/Cu-IMCs at different welding speeds. (**a**) 800 rpm, 60 mm/min, FSLW, (**b**) 800 rpm, 80 mm/min, FSLW, (**c**) 800 rpm, 100 mm/min, FSLW, (**d**) 800 rpm, 60 mm/min, UFSLW, (**e**) 800 rpm, 80 mm/min, UFSLW, (**f**) 800 rpm, 100 mm/min, UFSLW.

In order to confirm the compound composition, as shown in Figures 6 and 7, the SEM images of IMCs under 800 rpm–60 mm/min were selected for EDS spot scanning (points A–E on each IMC layer) to determine the composition. The Al/Cu interface of the FSLW process at 800 rpm–60 mm/min generated three layers of IMCs, as shown in Figure 6a. For each layer of IMC, it can be inferred that the IMC layer adjacent to the Al side (point A) is the Al_2Cu phase, the middle layer (point B) is the AlCu phase, and the layer adjacent to the Cu side (point C) is the Al_4Cu_9 phase. The results are in agreement with that of Tan et al. [37]. Meanwhile, in Figures 6b and 7b, the IMC layers adjacent to the Al side (point D) and Cu side (point E) were identified as the Al_2Cu and Al_4Cu_9 phases for UFLSW, respectively. From the results of EDS spot scanning, it can be inferred that the AlCu phase was restrained with the acoustic action. It is also obvious that the copper interred in the Al side changed from blocks to particles with uniform distribution. The size of aluminum particles interred in the copper side also reduced. The reason is that the ultrasonic softening effect promoted the plastic flow ability of Al/Cu materials and, with the mechanical coupling action of the ultrasonic vibration and the stirring shear action of the tool, the particles were scattered.

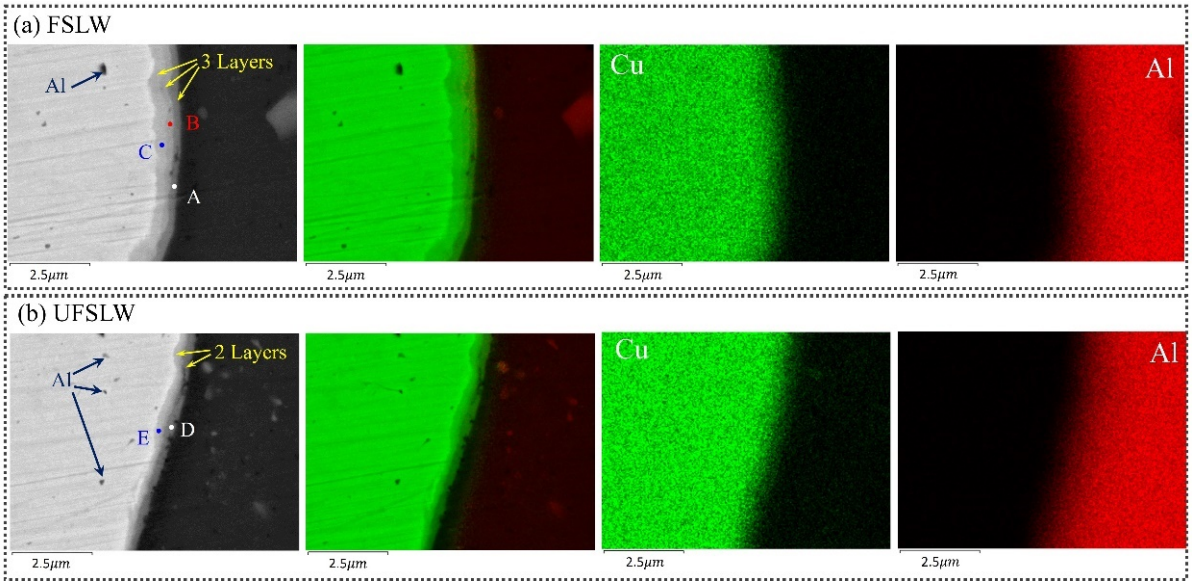

Figure 6. Comparison of the IMCs and element distribution on the Al/Cu interfaces at (**a**) 800 rpm, 60 mm/min of FSLW process, and (**b**) 800 rpm, 60 mm/min of UFSLW process. The points A, B, C, D and E are the positions for the EDS spot scanning.

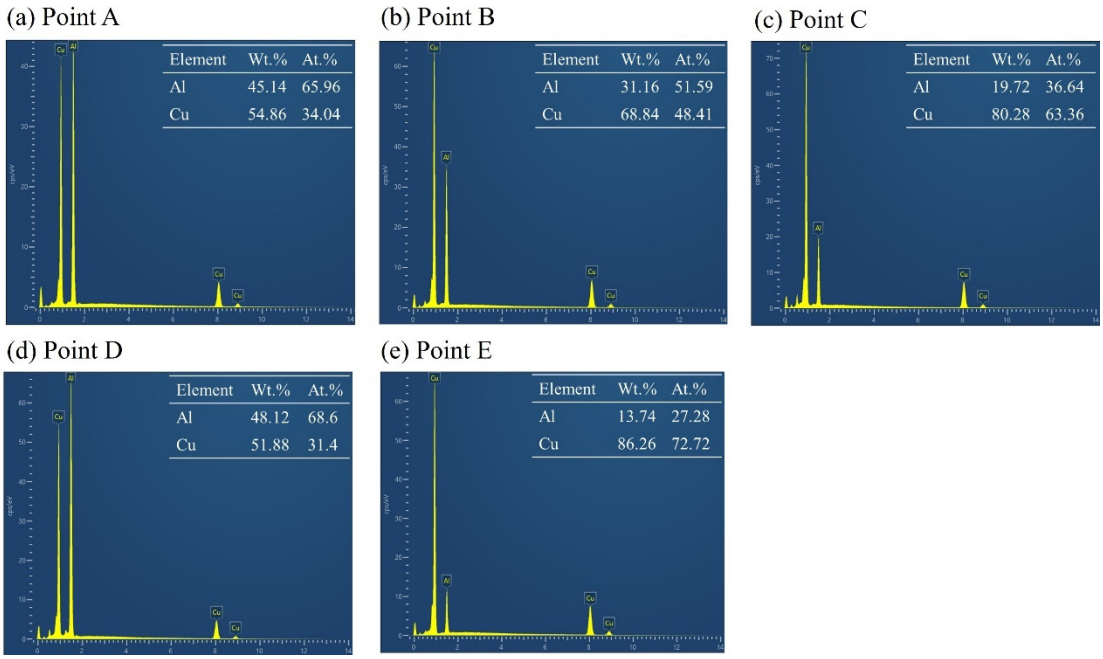

Figure 7. (**a**–**c**) EDS spot scanning results at the marked points A~C in Figure 6a for FSLW process at 800 rpm and 60 mm/min, and (**d**,**e**) EDS spot scanning results at the marked points D and E in Figure 6b for UFSLW process at 800 rpm and 60 mm/min.

As shown in Figure 8, the average layer thicknesses of compounds under different parameters in Figure 5 were measured and compared. At the welding speed of 60 mm/min, the effect of reducing IMC layer thickness by ultrasound is the most remarkable, and the IMC layer thickness was reduced by 42%. When the welding speed was increased to 100 mm/min, IMCs were 29% thinner than in the 60 mm/min condition. It can be concluded that applying ultrasonic field can reduce the thickness of IMCs more effectively compared with adjusting welding parameters.

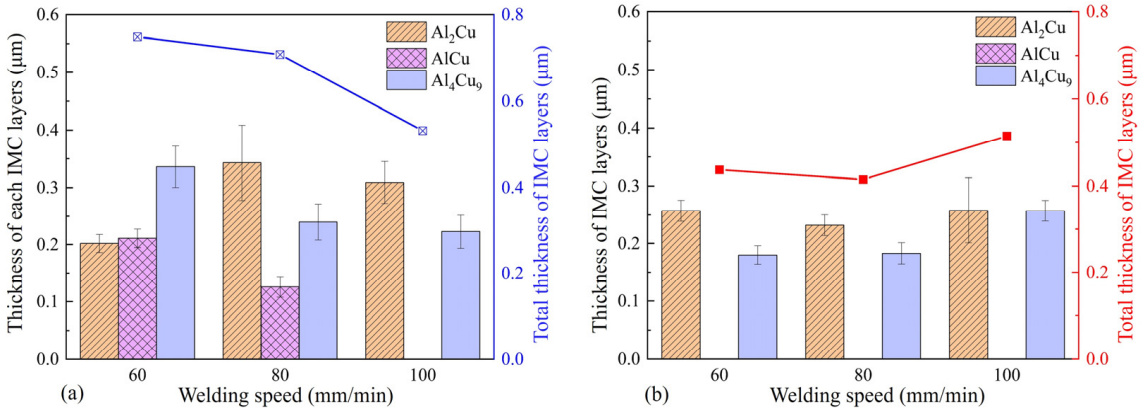

Figure 8. Comparison of thickness of Al/Cu−IMCs for (**a**) FSLW process and (**b**) UFSLW process under different welding speeds.

The influence of ultrasound on the heat generation and plastic flow in the Al/Cu plastic zone will change the formation environment of Al/Cu-IMCs. In order to confirm the formation order of Al/Cu-IMCs, the effective heat of formation (EHF) was calculated. The formation of specific Al/Cu-IMCs was based on the concentrations of copper and aluminum. When the Al/Cu concentrations match one kind of Al/Cu-IMC, the most negative effective Gibbs free energy could release the most energy to generate this kind of Al/Cu-IMC on the interface [38]. So, the more negative the effective Gibbs free energy, the more easily the corresponding IMC would be formed. The effective Gibbs free energy ΔG_e can be calculated with the following equation:

$$\Delta G_e = \frac{C_{eff}}{C_0} \Delta G_0 \quad (1)$$

where C_{eff} and C_0 are the effective concentration and concentration in the given compound of the limiting elements, and ΔG_0 is the Gibbs free energy required to form the given phase. The EDS point scanning in Figure 7 was used for analysis, and the temperature was estimated to be about 700 K. The results are shown in Table 2 and Figure 9.

Table 2. Calculated ΔG_e of Points A, C, D, and E in Figure 6 for the FSLW and UFSLW processes.

Effective Concentrations			Limiting Element				ΔG_e (kJ/mol)			
Phases	**Compound Composition**	**ΔG_0 (J/mol)**	**Point A $Al_{65.96}Cu_{34.04}$**	**Point C $Al_{36.64}Cu_{63.36}$**	**Point D $Al_{68.6}Cu_{31.4}$**	**Point E $Al_{27.28}Cu_{72.72}$**	**Point A**	**Point C**	**Point D**	**Point E**
Al_2Cu	$Al_{67}Cu_{33}$	−15,826.2 + 2.3T	Al	Al	Cu	Al	−13.9	−7.8	−13.5	−5.8
AlCu	$Al_{50}Cu_{50}$	−20,496.8 + 1.6T	Cu	Al	Cu	Al	−13.2	−14.2	−12.2	−10.6
Al_3Cu_4	$Al_{43}Cu_{57}$	−20,197.4 + 1.9T	Cu	Al	Cu	Al	−11.3	−16.1	−10.4	−12.0
Al_2Cu_3	$Al_{40}Cu_{60}$	−20,137.8 + 1.6T	Cu	Al	Cu	Al	−10.8	−17.4	−9.9	−13.0
Al_4Cu_9	$Al_{31}Cu_{69}$	−19,707.1 + 1.6T	Cu	Cu	Cu	Al	−9.2	−17.1	−8.5	−16.4

Comparing points A and D with or without ultrasound, the Al_2Cu phase near the Al side presented the most negativity, corresponding to the first phase generated. Similarly, at points C and E, Al_4Cu_9 phase was the first phase near the copper side. This indicated that the application of ultrasound cannot change the generation order of Al/Cu−IMCs, which was consistent with Huang et al. [39] and our previous research on aluminum–copper FSW [36]. However, comparing Figure 9a,c, the absolute value of EHF was reduced with ultrasonic effect, as well as in comparison of Figure 9b,d. The results indicated that the phase generation was delayed, which may be because ultrasound inhibited the generation of IMCs. Therefore, under the action of ultrasound, the layer thickness of IMCs was reduced

and the types of Al/Cu−IMC were reduced. With the reduction in the absolute value of ΔG_e for the AlCu phase, it could not release enough energy to generate AlCu phase. Furthermore, under the change in rheological state of local materials under ultrasonic vibration, the Al/Cu phase disappeared in the UFSLW process.

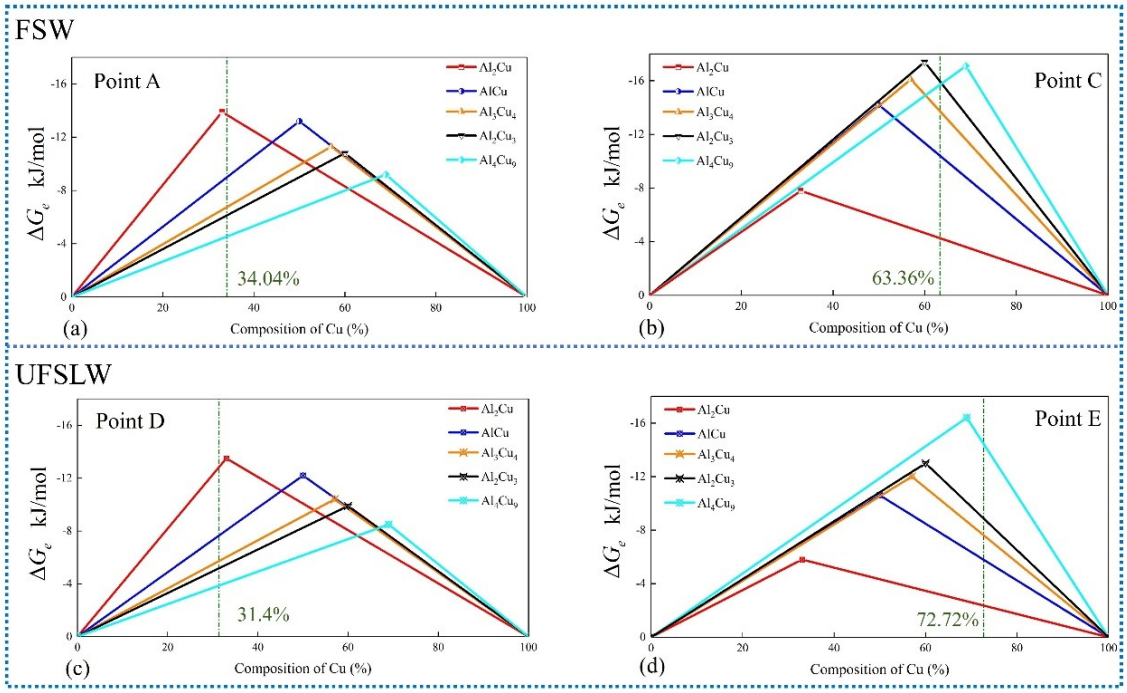

Figure 9. Comparison of the effective Gibbs free energy for the formation of Al/Cu−IMCs phases: (**a**) $Al_{65.96}Cu_{34.04}$ at point A in FSLW process under 800 rpm–60 mm/min, (**b**) $Al_{36.64}Cu_{63.36}$ at point C in FSLW process under 800 rpm–60 mm/min, (**c**) $Al_{68.6}Cu_{31.4}$ at point D in UFSLW process under 800 rpm–60 mm/min, and (**d**) $Al_{27.28}Cu_{72.72}$ at point E in UFSLW process under 800 rpm−60 mm/min. Points A, C, D, E correspond to Figure 6.

In addition, the tensile strengths of the joints under different welding speeds with and without UV are compared in Figure 10. It is clear that the tensile strength is improved with the increasing of welding velocity for both FSLW and UFSLW processes. And the ultrasound effectively improved the mechanical properties and elongation of the Al/Cu−lap joints under different welding speeds. The mechanism is related to the acoustic depression effect on the growth of IMCs. Moreover, it is clear that when the welding speed was increased from 80 mm/min to 100 mm/min, the effect of improving the tensile strength of the joint was higher than that of increasing the welding speed from 60 mm/min to 80 mm/min. This is because, when the welding speed was raised to 100 mm/min, the formation of AlCu phase was suppressed, and the thinning of the compound layer was the most obvious. Also, the heat input and temperature are reduced with the increasing of the welding speed, which also inhibited the formation of IMCs. When the AlCu phase was generated in the FSLW process, the effect of ultrasonic assistance on tensile strength was very significant. There is no mesophase AlCu in the joint at 100 mm/min in the FSLW process, and there is little difference in the tensile strength of the joint in Figure 10c.

As shown in Figure 11, the distributions of microhardness values measured along the thickness direction of the weld center were compared. For different welding speeds, the hardness had little change. After ultrasonic application, the hardness of the weld nugget zone decreased slightly. The reason is that the ultrasound can inhibit the generation and development of IMCs and reduce the content of IMCs in the nugget zone. Therefore, with the decrease in brittle-hard phase, the hardness of the joint decreased slightly.

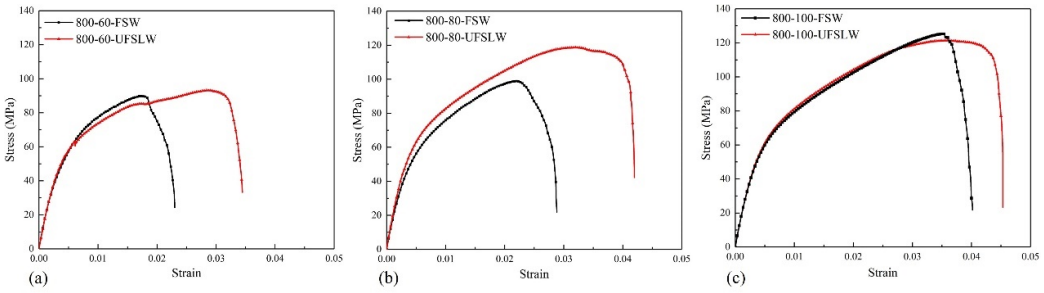

Figure 10. Comparison of the tensile strength of the joints under different welding speeds with and without ultrasonic vibration assistance. (**a**) 800 rpm, 60 mm/min, (**b**) 800 rpm, 80 mm/min, (**c**) 800 rpm, 100 mm/min.

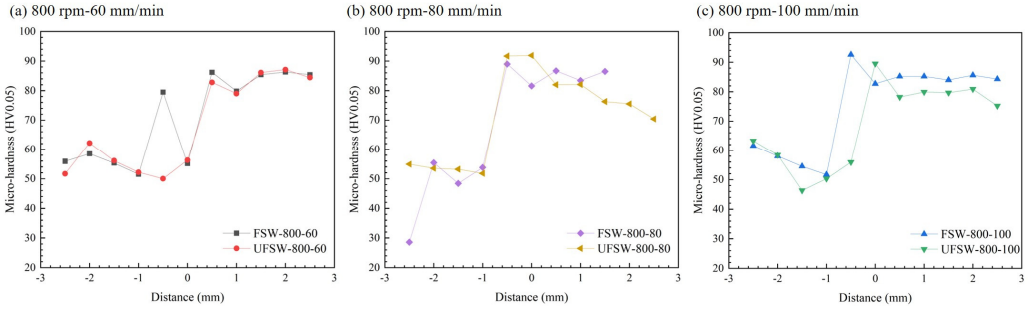

Figure 11. Comparison of the microhardness of the joints under different welding speeds with and without ultrasonic vibration assistance. (**a**) 800 rpm, 60 mm/min, (**b**) 800 rpm, 80 mm/min, (**c**) 800 rpm, 100 mm/min.

4. Conclusions

In this paper, the ultrasonic vibration was coupled with the Al/Cu friction stir lap welding process. And the depressive effects of ultrasound on Al/Cu−IMCs were elucidated with the variation of welding speed through macro–microstructure evolution analysis. The main conclusions are summarized:

1. The effect of welding speed on material plastic flow is different from the action mechanism of ultrasound. With the increase in welding speed, the heat generation decreases, and the shearing effect of the tool on the bottom copper increases, forming more Al/Cu staggered and interlocking layered structures. Meanwhile, the ultrasonic softening promotes the plastic deformation and reduces the deformation resistance of copper. Thus, the mechanical interlocking structure of aluminum and copper layers increases, and the size of copper particles/blocks entering the aluminum side decreases under ultrasonic effects.
2. The ultrasonic assistance and the increase in welding speed can both improve the uniformity and continuity of the IMC layer. The IMC layer thickness is reduced by about 42% under ultrasonic effect at the welding speed of 60 mm/min. When the welding speed is increased to 100 mm/min, IMCs are 29% thinner than at 60 mm/min. At three welding speeds, ultrasound can inhibit the formation of AlCu phase. Meanwhile, the welding speed must be increased to 100 mm/min to inhibit the formation of AlCu phase. Compared with increasing welding speed, applying ultrasonic field can reduce the IMCs more effectively.
3. The tensile strength and elongation of aluminum–copper lap joints can be improved by applying ultrasound or increasing the welding speed. The reasons are related to the acoustic depression effect on the growth of IMCs. Also, the heat input and temperature are reduced with the increasing of the welding speed, which also inhibited the formation of IMCs.

4. When AlCu phase appears in the joint, the effect of increasing welding speed on improving the tensile strength of the joint is not as significant as that of ultrasound. When the speed is increased to 100 mm/min, the formation of AlCu phase is inhibited, and the tensile strength of the joint is significantly improved without ultrasound.

Author Contributions: Conceptualization, X.Y. and A.F.; Methodology, Y.Z., Z.L. and X.Y.; Software, W.Z. and Y.Z.; Validation, Z.L., X.Y. and J.W.; Formal analysis, Z.L. and J.W.; Investigation, Y.Z. and Z.L.; Resources, J.W. and A.F.; Data curation, Z.L. and J.W.; Writing—original draft, W.Z. and Y.Z.; Writing—review and editing, F.W. and H.H.; Visualization, A.F. and Huan He; Supervision, A.F. and F.W.; Project administration, A.F.; Funding acquisition, W.Z. and X.Y. All authors have read and agreed to the published version of the manuscript.

Funding: This research was funded by the National Natural Science Foundation of China grant number [No. 52205423 and No. 52471210].

Data Availability Statement: The original contributions presented in the study are included in the article, further inquiries can be directed to the corresponding authors.

Acknowledgments: The authors acknowledge financial support from the National Natural Science Foundation of China (Grant No. 52205423 and No. 52471210).

Conflicts of Interest: The authors declare that they have no known competing financial interests or personal relationships that could have appeared to influence the work reported in this paper.

References

1. Siddharth, S.; Senthilkumar, T.; Chandrasekar, M. Development of processing windows for friction stir spot welding of aluminum Al5052/copper C27200 dissimilar materials. *Trans. Nonferrous Met. Soc. China* **2017**, *27*, 1273–1284. [CrossRef]
2. Kumar, M.; Das, A.; Ballav, R. Influence of interlayer on microstructure and mechanical properties of friction stir welded dissimilar joints: A review. *Mater. Today Proc.* **2020**, *26*, 2123–2129. [CrossRef]
3. Sadeghian, A.; Iqbal, N. A review on dissimilar laser welding of steel-copper, steel-aluminum, aluminum-copper, and steel-nickel for electric vehicle battery manufacturing. *Opt. Laser Technol.* **2022**, *146*, 107595. [CrossRef]
4. Fortunato, A.; Ascari, A. Laser welding of thin copper and aluminum sheets: Feasibility and challenges in continuous-wave welding of dissimilar metals. *Lasers Manuf. Mater. Process.* **2019**, *6*, 136–157. [CrossRef]
5. Chen, H.; Bi, G.; Nai, M.L.S.; Wei, J. Enhanced welding efficiency in laser welding of highly reflective pure copper. *J. Mater. Process. Technol.* **2015**, *216*, 287–293. [CrossRef]
6. Yusefi, A.; Kokabi, H.A.; Abedini, R.; Fartashvand, V.; Allahverdizadeh, V. Microstructure evolution and mechanical properties analysis in dissimilar ultrasonic metal welding of aluminum to copper. *J. Mater. Res. Technol.* **2024**, *30*, 2922–2935. [CrossRef]
7. Zhou, L.; Li, G.; Zhang, R.; Zhou, W.; He, W.; Huang, Y.; Song, S. Microstructure evolution and mechanical properties of friction stir spot welded dissimilar aluminum-copper joint. *J. Alloys Compd.* **2019**, *775*, 372–382. [CrossRef]
8. Fujii, H.; Endo, H.; Sato, Y.; Kokawa, H. Interfacial microstructure evolution and weld formation during ultrasonic welding of Al alloy to Cu. *Mater. Charact.* **2018**, *139*, 233–240. [CrossRef]
9. Isa, M.S.M.; Moghadasi, K.; Ariffin, M.A.; Raja, S.; bin Muhamad, M.R.; Yusof, F.; Jamaludin, M.F.; bin Yusoff, N.; bin Ab Karim, M.S. Recent research progress in friction stir welding of aluminium and copper dissimilar joint: A review. *J. Mater. Res. Technol.* **2021**, *15*, 2735–2780. [CrossRef]
10. Yan, S.; Li, Z.Y.; Song, L.L.; Zhang, Y.Q.; Wei, S.Z. Research and development status of laser micro-welding of aluminum-copper dissimilar metals: A review. *Opt. Lasers Eng.* **2023**, *161*, 107312. [CrossRef]
11. Zhou, J.B.; He, D.J.; Zhang, R. Effect of pin offset on interface evolution and fracture behavior of aluminum/copper dissimilar friction stir welded. *Mater. Today Commun.* **2023**, *37*, 107585. [CrossRef]
12. Su, h.; Zhao, Q.Z.; Chen, J.; Wu, C.S. Evolutions of material flow and intermetallic compounds, and the correlations with mechanical properties of dissimilar Al/Cu friction stir welding joints. *J. Mater. Sci.* **2022**, *57*, 20485–20502. [CrossRef]
13. Zhang, W.; Shen, Y.; Yan, Y.; Gou, W.; Gou, G. Microstructure characterization and mechanical behavior of dissimilar friction stir welded Al/Cu couple with different joint configurations. *Int. J. Adv. Manuf. Technol.* **2018**, *94*, 1021–1030. [CrossRef]
14. Zhang, H.J.; Zhang, B.X.; Li, C.; Wang, Y.L.; Gao, Q.Z. Strengthening characteristic and mechanism of AlCoCrFeNi high-entropy alloy particles for Al-Cu dissimilar friction stir lap welded joint. *Mater. Charact.* **2023**, *203*, 113153. [CrossRef]
15. Saeid, T.; Abdollah-zadeh, A.; Sazgari, B. Weldability and mechanical properties of dissimilar aluminum-copper lap joints made by friction stir welding. *J. Alloys Compd.* **2010**, *490*, 652–655. [CrossRef]
16. Li, J.; Tang, F.; Paidar, M. Modified friction stir clinching-brazing of brass to AA5083 aluminum alloy using Zn interlayer. *Arch. Civ. Mech. Eng.* **2021**, *21*, 13. [CrossRef]
17. Maity, D.; Racherla, V. Effect of SiC interlayer on microstructure and joint strength of Cu-Al welds obtained using a new friction processing method. *CIRP J. Manuf. Sci. Technol.* **2024**, *52*, 73–85. [CrossRef]

18. Tong, L.; Xie, J.; Liu, L.; Chang, G.; Ojo, O.O. Microscopic appraisal and mechanical behavior of hybrid Cu/Al joints fabricated via friction stir spot welding-brazing and modified friction stir clinching-brazing. *J. Mater. Res. Technol.* **2020**, *9*, 13239–13249. [CrossRef]
19. Paidar, M.; Ashraff Ali, K.S.; Mohanavel, V.; Mehrez, S.; Ravichandran, M.; Ojo, O.O. Weldability and mechanical properties of AA5083-H112 aluminum alloy and pure copper dissimilar friction spot extrusion welding-brazing. *Vacuum* **2021**, *187*, 110080. [CrossRef]
20. You, J.Q.; Zhao, Y.Q.; Dong, C.L. Microstructural evolution and mechanical properties of the Al-Cu dissimilar joint enhanced by stationary-dynamic shoulder friction stir welding. *J. Mater. Process. Technol.* **2022**, *300*, 117402. [CrossRef]
21. Ji, H.; Deng, T.L.; Xu, H.Y.; Yin, X.X.; Zhang, T.; Wang, W.Q.; Dong, H.G.; Wang, T.Y.; Wu, J.P. Numerical modeling for the mechanism of shoulder and pin features affecting thermal and material flow behavior in friction stir welding. *J. Mater. Res. Technol.* **2022**, *21*, 662–678. [CrossRef]
22. Chen, G.; Li, H.; Wang, G.; Guo, Z.; Zhang, S.; Dai, Q.; Wang, X.; Zhang, G.; Shi, Q. Effects of pin thread on the in-process material flow behavior during friction stir welding: A computational fluid dynamics study. *Int. J. Mach. Tools Manufact.* **2017**, *124*, 12–21. [CrossRef]
23. Su, H.; Xue, L.; Wu, C.S. Optimizing the tool pin with three flats in friction stir welding of aluminum alloy. *Int. J. Adv. Manuf. Technol.* **2020**, *108*, 721–733. [CrossRef]
24. Mehta, K.P.; Badheka, V.J. Hybrid approaches of assisted heating and cooling for friction stir welding of copper to aluminum joints. *J. Mater. Process. Technol.* **2017**, *239*, 336–345. [CrossRef]
25. Hu, Y.Y.; Liu, H.J.; Du, S.S. Achievement of high-strength 2219 aluminum alloy joint in a broad process window by ultrasonic enhanced friction stir welding. *Mater. Sci. Eng. A-Struct.* **2021**, *804*, 140587. [CrossRef]
26. Zhu, S.H.; Wang, N.Q.; Li, S.; Huang, G.; Ge, S.; Du, P.; Zhang, L.; Sun, Y.; Guan, S. Study on the materials flow, microstructure and mechanical properties of ultrasonic vibration-assisted friction stir weld of 1500 MPa martensitic steel. *Mater. Charact.* **2023**, *206*, 113409. [CrossRef]
27. Zhao, J.J.; Wu, C.S.; Shi, L.; Su, H. Evolution of microstructures and intermetallic compounds at bonding interface in friction stir welding of dissimilar Al/Mg alloys with/without ultrasonic assistance. *J. Mater. Sci. Technol.* **2023**, *139*, 31–46. [CrossRef]
28. Xie, L.; Xiao, X.; Zhu, X.; Fan, Y.; Jiang, C.; Song, Y. Influence mechanism of pin thread in friction stir welding of magnesium alloys based on the relationship between microstructure and mechanical properties. *J. Mater. Process. Technol.* **2023**, *312*, 117870. [CrossRef]
29. Zuo, Y.Y.; Gong, P.; Ji, S.D.; Li, Q.H.; Ma, Z.W.; Lv, Z. Ultrasound-assisted friction stir transient liquid phase spot welded dissimilar copper-aluminum joint. *J. Manuf. Process.* **2021**, *62*, 58–66. [CrossRef]
30. He, C.S.; Wang, T.; Zhang, Z.Q.; Qiu, C.P. Coupling effect of axial ultrasonic vibration and tool thread on the microstructure and properties of the friction stir lap welding joint of Al/Mg dissimilar alloys. *J. Manuf. Process.* **2022**, *80*, 95–107. [CrossRef]
31. Karrar, G.; Galloway, A.; Toumpis, A. Microstructural characterization and mechanical properties of dissimilar AA5083-copper joints produced by friction stir welding. *J. Mater. Res. Technol.* **2020**, *9*, 11968–11979. [CrossRef]
32. You, J.; Zhao, Y.; Dong, C.; Su, Y. Improving the microstructure and mechanical properties of Al-Cu dissimilar joints by ultrasonic dynamic-stationary shoulder friction stir welding. *J. Mater. Process. Technol.* **2023**, *311*, 117812. [CrossRef]
33. Su, H.; Zhao, Q.; Chen, J.; Wu, C. Homogenizing the intermetallic compounds distribution in Al/Cu dissimilar friction stir welding joint with the assistance of ultrasonic vibration. *Mater. Today Commun.* **2022**, *31*, 103643. [CrossRef]
34. Chowdhury, I.; Sengupta, K.; Maji, K.K.; Roy, S.; Ghosal, S. Investigation of mechanical properties of dissimilar joint of Al6063 aluminium alloy and C26000 copper alloy by ultrasonic assisted friction stir welding. *Mater. Today Proc.* **2022**, *50*, 1527–1534. [CrossRef]
35. Thoma, M.; Wagner, G.; Straß, B.; Wolter, B.; Benfer, S.; Fürbeth, W. Ultrasound enhanced friction stir welding of aluminum and steel: Process and properties of EN AW 6061/DC04-Joints. *J. Mater. Sci. Technol.* **2017**, *34*, 163–172. [CrossRef]
36. Zhao, W.Z.; Zhu, Y.L.; Liu, Z.X.; Fu, A.; He, H. Mechanism of ultrasonic effects on thermal-stress field in Cu/Al-FSW process. *Int. J. Mech. Sci.* **2024**, *270*, 109101. [CrossRef]
37. Tan, C.W.; Jiang, Z.G.; Li, L.Q.; Chen, Y.B.; Chen, X.Y. Microstructural evolution and mechanical properties of dissimilar Al-Cu joints produced by friction stir welding. *Mater. Des.* **2013**, *51*, 466–473. [CrossRef]
38. Mao, Y.; Qin, D.Q.; Xiao, X.; Wang, X.C.; Fu, L. Achievement of high-strength Al/Cu dissimilar joint during submerged friction stir welding and its regulation mechanism of intermetallic compounds layer. *Mater. Sci. Eng. A* **2023**, *865*, 144164. [CrossRef]
39. Hang, C.J.; Wang, C.Q.; Mayer, M.; Tian, Y.H.; Zhou, Y.; Wang, H.H. Growth behavior of Cu/Al intermetallic compounds and cracks in copper ball bonds during isothermal aging. *Microelectron. Reliab.* **2008**, *48*, 416–424. [CrossRef]